JCB Journal of Cell Biology

ARTICLE

Cell polarity–dependent centrosome separation in the *C. elegans* embryo

Alexandra Bondaz[1,2], Luca Cirillo[1,2], Patrick Meraldi[1,2], and Monica Gotta[1,2,3]

In animal cells, faithful chromosome segregation depends on the assembly of a bipolar spindle driven by the timely separation of the two centrosomes. Here we took advantage of the highly stereotypical cell divisions in *Caenorhabditis elegans* embryos to identify new regulators of centrosome separation. We find that at the two-cell stage, the somatic AB cell initiates centrosome separation later than the germline P1 cell. This difference is strongly exacerbated by the depletion of the kinesin-13 KLP-7/MCAK, resulting in incomplete centrosome separation at NEBD in AB but not P1. Our genetic and cell biology data indicate that this phenotype depends on cell polarity via the enrichment in AB of the mitotic kinase PLK-1, which itself limits the cortical localization of the dynein-binding NuMA orthologue LIN-5. We postulate that the timely separation of centrosomes is regulated in a cell type–dependent manner.

Introduction

Efficient formation of a bipolar spindle is essential for the proper segregation of the genetic information into the two daughter cells. The main microtubule organizing centers, the centrosomes, are nonessential for mitosis; nevertheless, whenever they are present, they play a dominant role in bipolar spindle assembly. Failure or a delay in centrosome separation can lead to chromosomes segregation defects, aneuploidy, and cell death (Meraldi, 2016). As a consequence, mitosis and centrosome separation are attractive targets for anti-cancer therapy (Mazzorana et al., 2011).

In human cells, the timing of centrosome separation is variable: in the prophase pathway, centrosome separation occurs before nuclear envelope breakdown (NEBD) and the bipolar spindle is established directly; in the prometaphase pathway, the two centrosomes are juxtaposed at NEBD, resulting in a monopolar spindle configuration that only later becomes bipolar (Mardin et al., 2013; Rattner and Berns, 1976; Rosenblatt, 2005; Rosenblatt et al., 2004; Toso et al., 2009; Waters et al., 1993). Cells using the prometaphase pathway tend to have a higher incidence of chromosome mis-segregation, indicating a need for timely centrosome separation (Kaseda et al., 2012; McHedlishvili et al., 2012; Silkworth et al., 2012). The existence of the prometaphase pathway is, however, not a tissue culture artifact, since centrosomes of dividing keratinocytes are still anchored at the apical membrane at NEBD, and centrosome separation is initiated only during prometaphase (Poulson and Lechler, 2010). Overall this high plasticity in timing implies that centrosome separation must be under the control of several players acting in parallel.

In most organisms, the microtubule motor kinesin-5 (Eg-5 in humans) is essential for centrosome separation (Ferenz et al., 2010). Tetrameric Eg-5 cross-links anti-parallel microtubules and pushes the centrosomes apart by sliding toward the microtubule plus ends (Kapitein et al., 2005). In human cells, Eg-5 impairment by siRNA, antibodies, or chemical inhibitors results in monopolar spindle formation (Blangy et al., 1995; Elbashir et al., 2001; Mayer et al., 1999). Nevertheless, other microtubule-associated proteins are involved in centrosome separation: another tetrameric microtubule motor, kinesin-12 (Kif15 in humans), accelerates centrosome separation and becomes essential when Eg-5 activity is partially inhibited (Drechsler et al., 2014; Tanenbaum et al., 2009; Vanneste et al., 2009). The microtubule minus end–directed dynein motor complex participates in centrosome separation in two ways: first, by pulling at the cell cortex on astral microtubules (Vaisberg et al., 1993; van Heesbeen et al., 2014) and by pulling centrosomes apart at the nuclear envelope (Raaijmakers et al., 2012); and finally, MCAK, a member of the kinesin-13 microtubule depolymerase family, becomes essential to keep centrosomes separated when Eg-5 is inhibited (van Heesbeen et al., 2017).

[1]Department of Cell Physiology and Metabolism, Faculty of Medicine, University of Geneva, Geneva, Switzerland; [2]Translational Research Centre in Onco-hematology, Faculty of Medicine, University of Geneva, Geneva, Switzerland; [3]Swiss National Centre for Competence in Research in Chemical Biology, University of Geneva, Geneva, Switzerland.

Correspondence to Patrick Meraldi: patrick.meraldi@unige.ch; Monica Gotta: monica.gotta@unige.ch.

Here, we aimed to identify new factors controlling centrosome separation. We took advantage of the *Caenorhabditis elegans* embryo as a model system since it is one of the rare organisms in which Eg-5, called BMK-1, is not essential to drive centrosome separation (Bishop et al., 2005). *C. elegans* embryos have very stereotypical divisions and exclusively use the prophase centrosome separation pathway (Hyman and White, 1987). It is, however, possible to partially delay centrosome separation when depleting the spindle positioning regulator Gα (De Simone et al., 2016; Gotta and Ahringer, 2001). Here, we show that depletion of the kinesin-13 KLP-7^{MCAK} leads to a strong centrosome separation defect in the anterior AB cell in two-cell embryos, but not in the posterior P1 cell. This defect is due to polarity-dependent cytoplasmic accumulation of the mitotic kinase Polo-like kinase 1 (PLK-1) in AB (Budirahardja and Gönczy, 2008; Nishi et al., 2008; Rivers et al., 2008). PLK-1 inhibits centrosome separation in AB by suppressing the cortical localization of the dynein-binding LIN-5^{NuMA} protein. We propose that cell polarity modulates centrosome separation via PLK-1 and LIN-5.

Results

Depletion of the microtubule depolymerase KLP-7^{MCAK} results in a centrosome separation defect in AB

To investigate the molecular mechanisms controlling bipolar spindle assembly in early *C. elegans* embryos, we recorded 4D time-lapse videos in a strain expressing YFP-α-tubulin and depleted the orthologues of proteins known to regulate centrosome separation in human cells: BMK-1, the Eg-5 orthologue; KLP-18, the orthologue of the kinesin-12 Kif15; and KLP-7, the MCAK orthologue. Visual inspection of the videos indicated that centrosomes in one-cell embryos depleted of BMK-1, KLP-18, and KLP-7 were separated at NEBD (Bishop et al., 2005; Grill et al., 2001; Saunders et al., 2007; Segbert et al., 2003; Srayko et al., 2005). In two-cell embryos, however, KLP-7 depletion resulted in a visible centrosome separation defect in the anterior AB cell, but not the posterior P1 cell (Fig. 1 A). We calculated the ratio of the 3D distance between the centrosomes and the diameter of the nucleus in the time frame just before NEBD of both AB and P1 (Fig. S1) to analyze this phenotype in a quantitative manner. A ratio of 1 indicated that the centrosomes are diametrically opposed at NEBD, whereas a lower ratio indicated a defect in centrosome separation. In control embryos, the centrosomes were diametrically opposed at NEBD in P1 (median = 0.97), whereas in AB, centrosomes were slightly less separated (median = 0.90; for statistical significance and P values in all figures, see Table S1; Fig. 1, A and B). This phenotype was not dependent on the strain, as it was observed in three different strain backgrounds (TH65, JCC483, and SA250; Table S2) and independently of an RNAi treatment (Fig. S1 D). In KLP-7–depleted embryos, centrosomes were much closer at NEBD in AB (median = 0.69) and somewhat closer in P1 (median = 0.90; Fig. 1, A and B). This strong centrosome separation defect in AB was also observed in three *klp-7* mutant alleles (Connolly et al., 2015; Gigant et al., 2017) and in two other strain backgrounds (Fig. S1 C and Fig. 1, C and D). In contrast, the extent of centrosome separation in AB and P1 cells of embryos depleted of BMK-1 or KLP-18 alone as well as in embryos codepleted of BMK-1 and KLP-18 was not statistically different from the one of control embryos (Fig. 1, A and B).

The centrosome separation defect in *klp-7* mutants could also be observed in the next division, as centrosome separation was incomplete in both ABa and ABp, the AB daughters (Fig. S1 E). In contrast, in P2, the germline precursor, centrosomes separated as in the WT P2. Finally, in EMS, even though the median extent of centrosome separation was statistically not significantly different from P2, we observed a higher variability, pointing to a less robust process (Fig. S1 E). We conclude that the microtubule depolymerase KLP-7 is required for efficient centrosome separation in AB, and generally in somatic cells. This suggests that the mechanisms of bipolar spindle assembly are cell type dependent.

Centrosome separation initiation is delayed in KLP-7–depleted embryos

KLP-7–depleted embryos have more stable and more numerous astral microtubules in one-cell embryos (Srayko et al., 2005), suggesting that the astral microtubules could generate a pushing force at the cell cortex that hampers centrosome separation. We first asked whether endogenously GFP-tagged KLP-7 (Gerson-Gurwitz et al., 2016) is differentially enriched in AB and P1 cells, which could explain the difference in centrosome separation seen after KLP-7 RNAi. KLP-7 was found at centrosomes and kinetochores and was not enriched in the anterior, consistent with previous reports (Fig. S1 F; Fadero et al., 2018; Oegema et al., 2001). We next tested whether KLP-7 depletion differentially affects microtubules at the cell cortex in AB and P1, i.e., whether its loss would lead to a higher stabilization of microtubules in AB than in P1. As a marker, we used a strain in which GFP is fused to EBP-2, a conserved protein that binds the plus ends of microtubules (Table S2; Srayko et al., 2005). We analyzed microtubule residency time and density at the cortex, and polymerization rate in AB and P1 cells of control and KLP-7–depleted embryos.

In unperturbed control embryos, the microtubule average residency time was higher in AB than in P1 (2.7 ± 0.05 s versus 2.1 ± 0.13 s; Fig. 2 A), whereas microtubule density and polymerization rate were not statistically different (Fig. 2, B and C). Consistent with its role as a microtubule depolymerase, KLP-7 depletion increased the cortical microtubule density in both AB and P1 (Fig. 2 B); however, it did not increase the density more in AB than P1; to the contrary, it dampened the difference in microtubule residency time (Fig. 2, A–C). These data suggest that the difference in centrosome separation behavior in AB compared with P1 in KLP-7–depleted embryos does not arise from a more efficient astral microtubule stabilization in AB.

To better understand the mechanistic origin of the centrosome separation defect, we next tracked the two centrosomes in WT and *klp-7* mutant two-cell embryos over time. We first asked whether the AB-specific centrosome separation defect in *klp-7* embryos was due to the shorter cell cycle of AB cells (reviewed in Rose and Gönczy, 2014). This was not the case, as in the majority of the *klp-7* mutant embryos (77%, n = 13), the centrosomes in P1 had already fully separated when the AB cell underwent NEBD (Videos 1, 2, and 3). Next, we plotted the average distance between the two centrosomes versus the timing

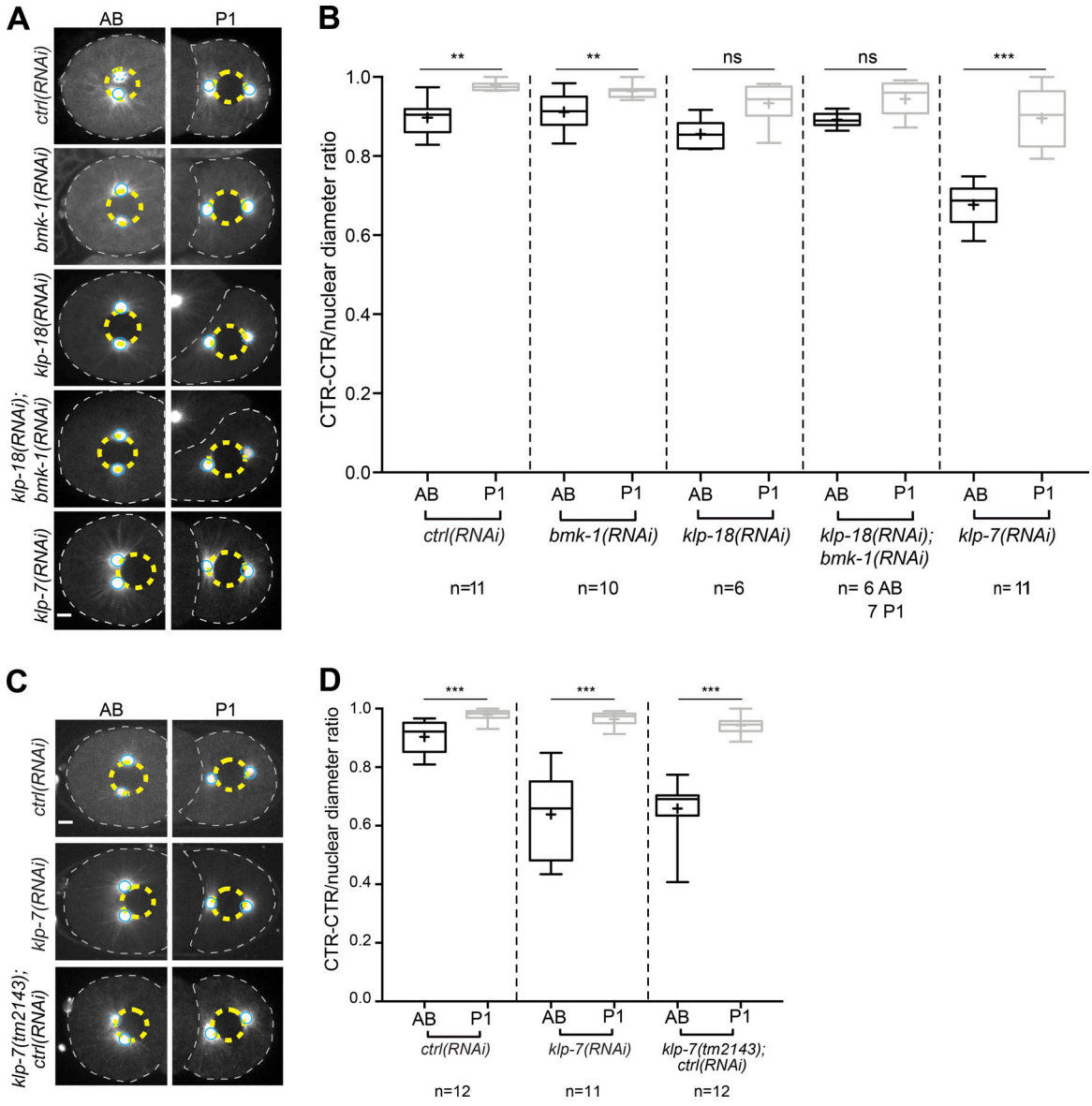

Figure 1. **Centrosome separation is defective in KLP-7 depleted embryos. (A)** Still images of the AB (left) and P1 cell (right) taken from time-lapse videos of a YFP::α-tubulin expressing strain (TH65) with the indicated depletions. For all the subsequent figures of centrosome position in AB and P1 throughout the paper, the images represent the maximum intensities of Z projection at the time point just before NEBD (15 s before NEBD), the dashed yellow line highlights the nucleus, centrosomes are highlighted with a blue circle (or dashed blue circle when not in focus), and the cell periphery is delimited by the dashed gray line. **(B)** Quantification of centrosome separation ratios (CTR-CTR) as illustrated in Fig. S1. In this and all subsequent figures, ratios are plotted as box plots (dark color in AB, light color in P1). **(C)** Still images of the AB (left) and P1 cell (right) taken from time-lapse videos of a GFP::β-tubulin expressing strain (JDU316, containing the *klp-7(tm2143)* deletion, and its parental strain, JCC483). **(D)** Quantification of centrosome separation ratios in the indicated genotypes. Scale bars, 5 µm. The number of cells/embryos analyzed is indicated at the bottom of the graph and the statistical test used is indicated in Table S1. **, P ≤ 0.01; ***, P ≤ 0.001.

of NEBD. This showed that the timing of centrosome separation initiation was different between AB and P1 cells: AB cells always initiated centrosome separation after P1 cells, and this delay was exacerbated in *klp-7* mutant embryos (Fig. 2 D). However, since in P1 the two centrosomes were often already separated, it was not possible to directly read out the centrosome separation velocities from this plot. We therefore extracted peak centrosome separation velocities from single-cell trajectories, when the inter-centrosome distances rapidly expand from 4 to 11 µm (Fig. S1 G). This analysis revealed that the centrosome separation velocities were neither significantly different between AB and P1 cells nor affected by loss of KLP-7 (Fig. S1 H). We conclude that loss of KLP-7 specifically delays the initiation of centrosome separation in AB.

The centrosome separation defect of KLP-7–depleted embryos depends on cell polarity

The AB and P1 blastomeres have a different fate: AB will give origin to somatic cells whereas P1 will give origin to somatic and germline cells (Sulston et al., 1983). The fate of AB and P1 is set

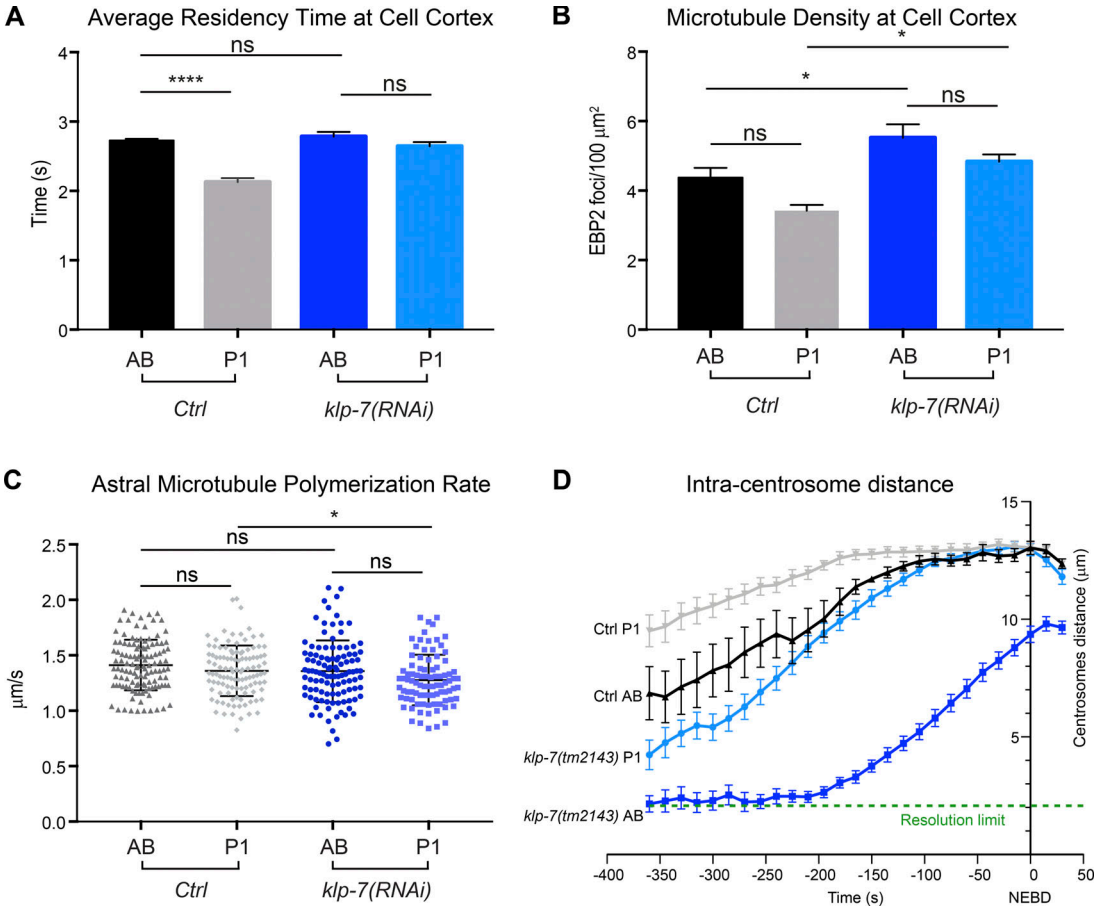

Figure 2. **Centrosome separation initiation is delayed in KLP-7 depleted embryos. (A)** Average residency time of microtubules at the cortex of AB and P1 in control and KLP-7–depleted embryos. Plus end microtubules were visualized using a strain expressing EBP2::GFP (TH66). In control, 1,303 tracks were measured in five AB cells and 770 tracks in five P1 cells; in KLP-7–depleted embryos, 1,786 tracks were measured in six AB cells and 1,372 tracks in five P1 cells. Each value corresponds to the mean residency time at the cortex in seconds ± SEM. **(B)** Quantification of cortical microtubule density. Tracking of microtubules was performed using a macro developed in ImageJ (see Materials and methods). Each value corresponds to the mean number of microtubules at the cortex in a surface of 100 µm² (n = 5 cells each). **(C)** Quantification of microtubule polymerization rate. The polymerization rate was based on EBP2 comets growing out from the centrosomes toward the cortex for at least 10 frames. A total of 110 microtubules were counted in WT AB cells, 90 in P1 cells, 120 in *klp-7(RNAi)* AB cells, and 111 in *klp-7(RNAi)* P1 cells (at least five cells each). **(D)** Tracking of the centrosome-to-centrosome distance over time in control embryos (n = 9 AB cells and 9 P1 cells) and in *klp-7(tm2143)* embryos (n = 17 AB cells and 15 P1 cells). T = 0 was set at NEBD for AB and P1, respectively. The green line indicates the minimal distance, under which it was not possible anymore to resolve the two centrosomes. Error bars represent SEM. The statistical test used is indicated in Table S1. *, P ≤ 0.05; ****, P ≤ 0.001.

during the division of the zygote and is under the control of the conserved partitioning defective (PAR) proteins, some of which localize asymmetrically along the anterior–posterior axis of the embryo. PAR-3, PAR-6, and PKC-3 are enriched at the anterior cortex, whereas PAR-2 and PAR-1 accumulate at the posterior cortex. PAR proteins control all aspects of asymmetric cell division from spindle positioning to the segregation of cytoplasmic factors and cell fate determinants (reviewed in Rose and Gönczy, 2014).

To investigate whether polarity itself controls the pattern of centrosome separation, we depleted PAR-2 or PAR-3 in control embryos and in the *klp-7(tm2143)* mutant. In PAR-2–depleted embryos, the anterior PAR-3 protein spreads around the entire embryo cortex; the first division is symmetric; and in the following division, both cells behave as WT AB. In contrast, after PAR-3 depletion, PAR-2 localizes all around the cortex; the first division is symmetric; and in the following division, both cells behave as WT P1 (Fig. 3 A). Centrosomes were separated at NEBD in both AB and P1 when PAR-2 or PAR-3 was depleted in the control strain (Fig. 3, B and C). If the centrosome separation defect in *klp-7* mutants depended on polarity, we expected that depleting PAR-2 in a *klp-7* mutant background should delay centrosome separation in P1 and that PAR-3 depletion should rescue centrosome separation in AB (Fig. 3 A). However, both PAR-2 and PAR-3 depletion impaired centrosome separation in both AB and P1 in the *klp-7(tm2143)* mutant (Fig. 3, B and C). Overall, this indicated that the centrosome separation defect of *klp-7* mutants depends on polarity, but not simply on cortical polarity, since depletion of both anterior and posterior PAR proteins leads to the same phenotype.

PLK-1 prevents centrosomes separation initiation in AB in KLP-7–depleted embryos

PAR proteins regulate the asymmetric segregation of cytoplasmic factors, which, in the *par* mutants, remain symmetric in the

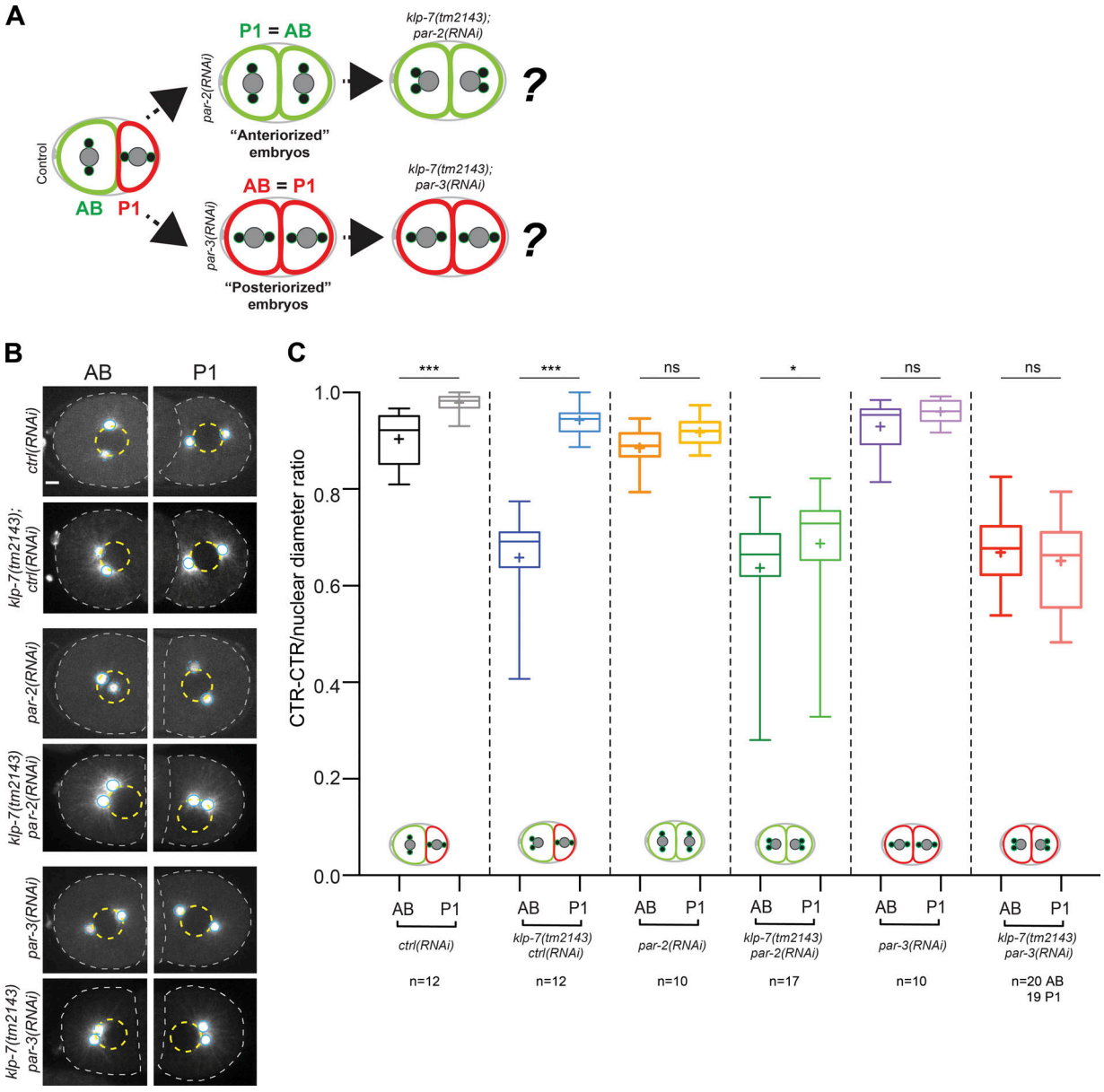

Figure 3. **The centrosome separation defect of KLP-7–depleted embryos depends on cell polarity. (A)** Schematic representation of the experiment: WT two-cell embryo with localization of anterior PAR proteins (in green) around AB and posterior PAR proteins (in red) around P1 on the left. Schematic representation of a *par-2(RNAi)* embryo on the top right and of a *par-3(RNAi)* embryo on the bottom right. The gray spheres represent the nuclei, and the black full circles are the centrosomes. **(B)** Still images of AB and P1 cells before NEBD taken from recordings of embryos treated with the indicated RNAi. JDU316 (containing the *klp-7(tm2143)* deletion) and its parental strain, JCC483, were used in this experiment. **(C)** Quantification of the centrosome separation ratios of the indicated genotypes. Model two-cell embryos indicate the polarity status (anterior in green; posterior in red) of the respective cell. Scale bar, 5 µm. The number of cells/embryos analyzed is indicated at the bottom of the graph and the statistical test used is indicated in Table S1. *, P ≤ 0.05; ***, P ≤ 0.001.

cytoplasm. An important factor is the mitotic kinase PLK-1, which regulates the function of the mitotic spindle at multiple steps of cell division. PLK-1 is enriched in the anterior cytoplasm of the one-cell embryo and preferentially segregated to AB in two-cell embryos (Budirahardja and Gönczy, 2008; Chase et al., 2000; Nishi et al., 2008; Rivers et al., 2008). We hypothesized that higher PLK-1 levels in AB might negatively impact centrosome separation.

To test this hypothesis, we asked whether PLK-1 impairment could rescue the AB centrosome separation defect in KLP-7–depleted embryos. We took advantage of a strain with a *plk-1* temperature-sensitive mutation, *plk-1(or683ts)*, and expressing tubulin fused to GFP. In *plk-1(or683ts)* embryos, centrosomes were separated at NEBD in both AB and P1, and depletion of KLP-7 in the control strain resulted in strong centrosome separation defects in AB (Fig. 4, A and B). This defect was rescued when KLP-7 was depleted in the *plk-1(or683ts)* (Fig. 4, A–C). The delay of centrosome separation initiation caused by KLP-7 depletion was also rescued by PLK-1 impairment (Fig. 4 D). This indicates that centrosome separation in AB is rescued when KLP-7 is

depleted in a *plk-1* temperature-sensitive background, suggesting that higher levels of PLK-1 at the anterior inhibit this process in a sensitized background such as KLP-7–depleted embryos.

We note that previous immunofluorescence studies had reported that PLK-1 levels are symmetric in AB and P1 in *par-2(RNAi)* or *par-3(RNAi)* embryos, but that the overall PLK-1 levels were lower, similar to WT P1, in *par-3(RNAi)* embryos (Budirahardja and Gönczy, 2008; Nishi et al., 2008; Rivers et al., 2008). Such low PLK-1 levels in *par-3(RNAi)* embryos were, however, inconsistent with the centrosome separation defects in AB and P1 cells of *klp-7(tm2143);par-3(RNAi)* embryos. We took advantage of a new strain in which endogenous PLK-1 has been labeled with GFP (hereafter called PLK-1::GFP; Martino et al., 2017) to reanalyze PLK-1 levels in AB and P1 after PAR-3 or PAR-2 depletion, at the time point right after division of the zygote, when centrosomes are still close (Fig. 4 E). In WT embryos, we observed an enrichment of PLK-1::GFP in AB compared with P1, as previously shown with antibodies and transgenic lines (Fig. 4, E and F; Budirahardja and Gönczy, 2008; Chase et al., 2000; Nishi et al., 2008; Rivers et al., 2008). In PAR-3–depleted embryos, PLK-1::GFP was equally distributed between AB and P1 (Fig. 4, E and F). Its levels were, however, intermediate between the levels observed in WT AB and P1 (Fig. 4, E and F). In PAR-2–depleted embryos, PLK-1::GFP levels were also intermediate between the levels observed in WT AB and P1 (Fig. 4, E and F), even though we observed a weak enrichment of PLK-1::GFP in AB compared with P1. This is consistent with the fact that polarity is established in PAR-2–depleted embryos, but maintenance is defective (Cuenca et al., 2003). We conclude that both PAR-2 and PAR-3 depletion result in intermediate levels of PLK-1 in AB and P1 in early two-cell embryos, consistent with the centrosome separation defect observed in both cells when combined with KLP-7 depletion.

To test whether symmetric distribution of PLK-1 is sufficient to induce centrosome separation defects in both AB and P1 in *klp-7* mutants, we depleted MEX-5 and MEX-6 (hereafter referred to as MEX-5/6). These two closely related proteins are enriched in the anterior cytoplasm in a PAR-dependent manner and bind PLK-1 to promote its enrichment in AB. In *mex-5(RNAi); mex-6(RNAi)* embryos, PAR proteins remain distributed asymmetrically along the anterior–posterior axis (Schubert et al., 2000; Cuenca et al., 2003; Cheeks et al., 2004), but the PLK-1 gradient is not established (Nishi et al., 2008; Rivers et al., 2008). When quantifying endogenously tagged PLK-1::GFP in *mex-5/6(RNAi)* embryos, we found similar levels in AB and P1, which were intermediate between the PLK-1 levels in WT AB and P1 (Fig. 5, A and B). MEX5/6 depletion did not affect centrosome separation on its own, but it impaired centrosome separation in both AB and P1 in the *klp-7(tm2143)* mutant (Fig. 5, C and D). We conclude that elevated levels of PLK-1 in AB inhibit centrosome separation when KLP-7 is depleted.

LIN-5 is required for the differential centrosome separation behaviors in AB and P1

We next speculated that PLK-1 could inhibit a factor in AB that promotes centrosome separation. Depletion of such a factor in a *klp-7* mutant background should impair centrosome separation in both AB and P1, and abolish the difference seen after inactivation of KLP-7 alone. To identify such a factor, we performed a candidate-based screen of proteins potentially implicated in centrosome separation in KLP-7 depletion/mutant background (Fig. 6 and Fig. S2). These include the microtubule motors KLP-18 and BMK-1, the dynactin orthologue DNC-1, as well as Gα and LIN-5 (the NuMA orthologue), which are required for cortical dynein recruitment (reviewed in di Pietro et al., 2016). Strikingly, LIN-5 impairment resulted in a centrosome separation defect in P1 as well, abolishing the difference between AB and P1 (Fig. 6, A and B). In contrast, KLP-18 and DNC-1 depletion further impaired centrosome separation in AB or, in the case of Gα, reduced the efficiency of centrosome separation in both AB and P1 (Fig. S2). This suggested that the presence of LIN-5 sets the difference between AB and P1. Consistent with this hypothesis, KLP-7 depletion in a *lin-5*–thermosensitive mutant strain (*lin-5(ev571ts)*) expressing GFP::β-tubulin (Park and Rose, 2008) impaired centrosome separation in AB and P1 to a similar extent (0.715 ± 0.0195 in AB versus 0.732 ± 0.0165 in P1). Moreover, *lin-5(ev571ts)* embryos displayed the same mild centrosome separation defect in AB and P1, abolishing any difference between the two cell types (0.802 ± 0.0208 in AB versus 0.791 ± 0.0128 in P1; Fig. 6, A and B).

LIN-5 is a dynein-binding coiled-coil protein that localizes to centrosomes and to the cortex (Couwenbergs et al., 2007; Lorson et al., 2000; Nguyen-Ngoc et al., 2007). To dissect whether the cortical or centrosomal pool of LIN-5 contributes to centrosome separation in a *klp-7(RNAi)* background, we depleted ASPM-1 (abnormal spindle-like, microcephaly associated), a centrosomal protein that is essential for LIN-5 recruitment to centrosomes (Fig. S3 A; van der Voet et al., 2009). Our results indicate that in *aspm-1(RNAi)* embryos, the centrosomes were separated in both AB and P1, and that *klp-7(tm2143);aspm-1(RNAi)* embryos behaved similarly to *klp-7(tm2143);ctrl(RNAi)* embryos (Fig. 6, C and D). We conclude that the cortical pool of LIN-5 is responsible for centrosome separation.

PLK-1 inhibits cortical LIN-5 recruitment in the AB cell

Our results suggested a model in which the higher PLK-1 levels in the AB cell prevent centrosome separation due to its inhibitory activity toward LIN-5. This is consistent with human cell data showing that hsPlk1 controls the cortical recruitment of the LIN-5 orthologue NuMA during mitosis (Sana et al., 2018). We therefore used a *C. elegans* strain in which LIN-5 is endogenously tagged with Neon Green (Heppert et al., 2018) to assess whether PLK-1 controls LIN-5 localization at the cell cortex in AB and P1. Using two independent methods, (1) we quantified the LIN-5::mNG signal along line profiles perpendicular to the cell cortex, and (2) we integrated the LIN-5::mNG intensity over an equal-sized stripe covering the cell cortex in AB and P1 (see also Materials and methods). With both methods, we found that in a WT background, LIN-5::mNG is present at higher levels in P1 when compared with AB (Fig. 7, A–C). Moreover, both datasets indicated that LIN-5::mNG levels were increased at the cell cortex in AB in PLK-1–depleted embryos (Fig. 7, A–C). In contrast, KLP-7 depletion did not affect cortical LIN-5 levels (Fig. S3, B–D). These

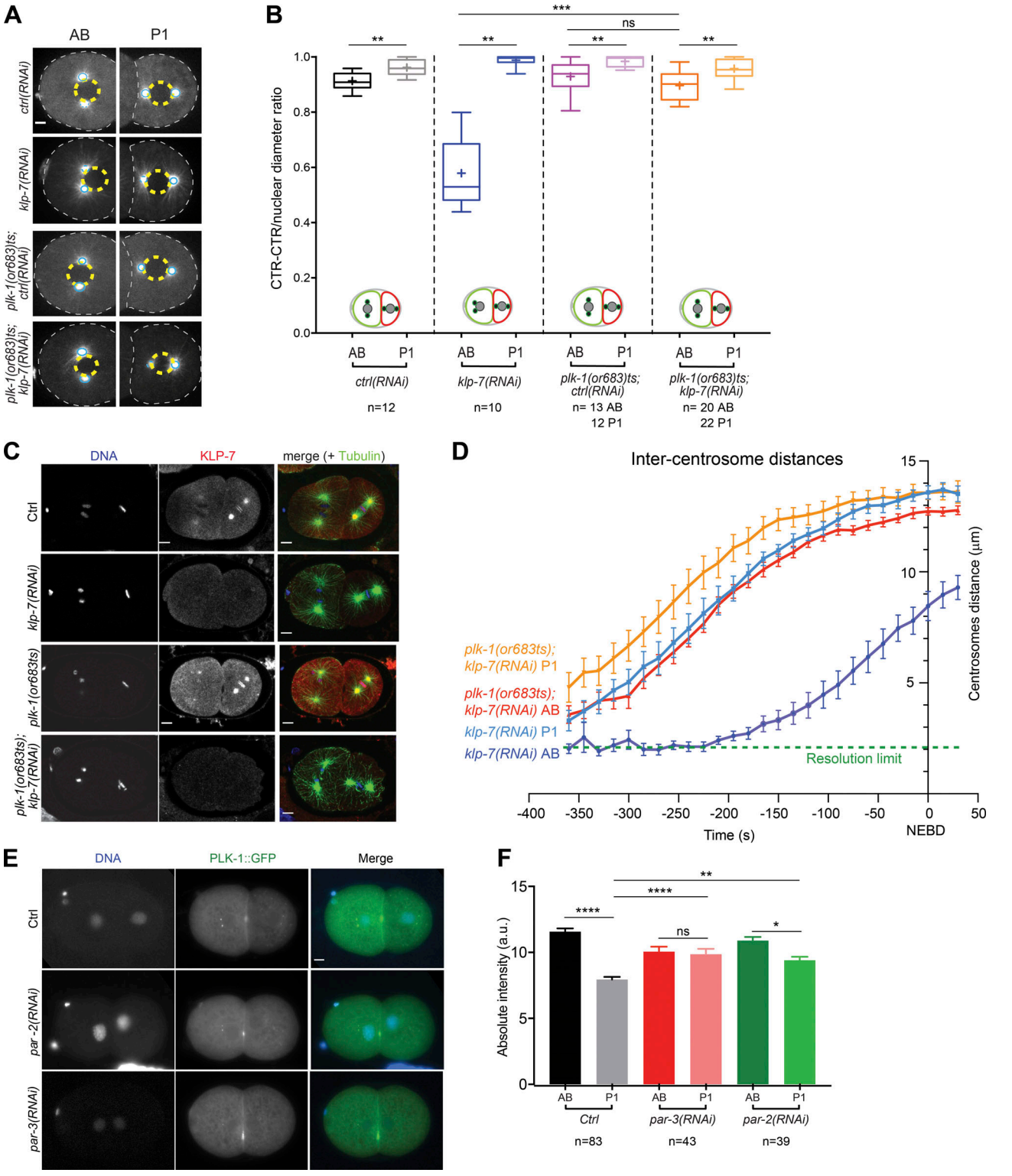

Figure 4. **The centrosome separation defect of KLP-7–depleted embryos is suppressed in *plk-1(or683ts)*. (A)** Still images from time-lapse recordings of AB and P1 cells from embryos of the indicated genotype. ZU655 (containing the *plk-1(or683ts)*) and its parental strain SA250 were used in this experiment. **(B)** Quantification of the centrosome separation ratios of the indicated genotypes. **(C)** Localization of KLP-7 in images of fixed embryos during the second division of the SA250 strain with or without *klp-7(RNAi)* and the ZU655 strain containing the *plk-1(or683ts)* allele with or without *klp-7(RNAi)*. KLP-7 localizes to the centrosomes, kinetochores, and cytoplasm. **(D)** Tracking of the centrosome-to-centrosome distance over time in *klp-7(RNAi)* embryos (*n* = 11 AB cells and 10 P1 cells) and in *plk1(or683ts);klp-7(RNAi)* embryos (*n* = 11 AB cells and 10 P1 cells). T = 0 was set at NEBD for AB and P1, respectively. The green line indicates the minimal distance, under which it was not possible anymore to resolve the two centrosomes. Error bars represent SEM. **(E)** Images of control, *par-3(RNAi)*, and *par-2(RNAi)* fixed early two-cell stage embryos expressing an endogenously tagged PLK-1::GFP. PLK-1 is observed at centrosomes, at the midbody, and in the cytoplasm. **(F)** Quantification of the absolute intensity of PLK-1::GFP in the cytoplasm of AB and P1 cells of control, *par-2(RNAi)*, or *par-3(RNAi)* embryos. Error bars indicate SEM. Scale bars, 5 µm. The number of cells/embryos analyzed is indicated at the bottom of the graph and the statistical test used is indicated in Table S1. *, P ≤ 0.05; **, P ≤ 0.01; ***, P ≤ 0.001; ****, P ≤ 0.001.

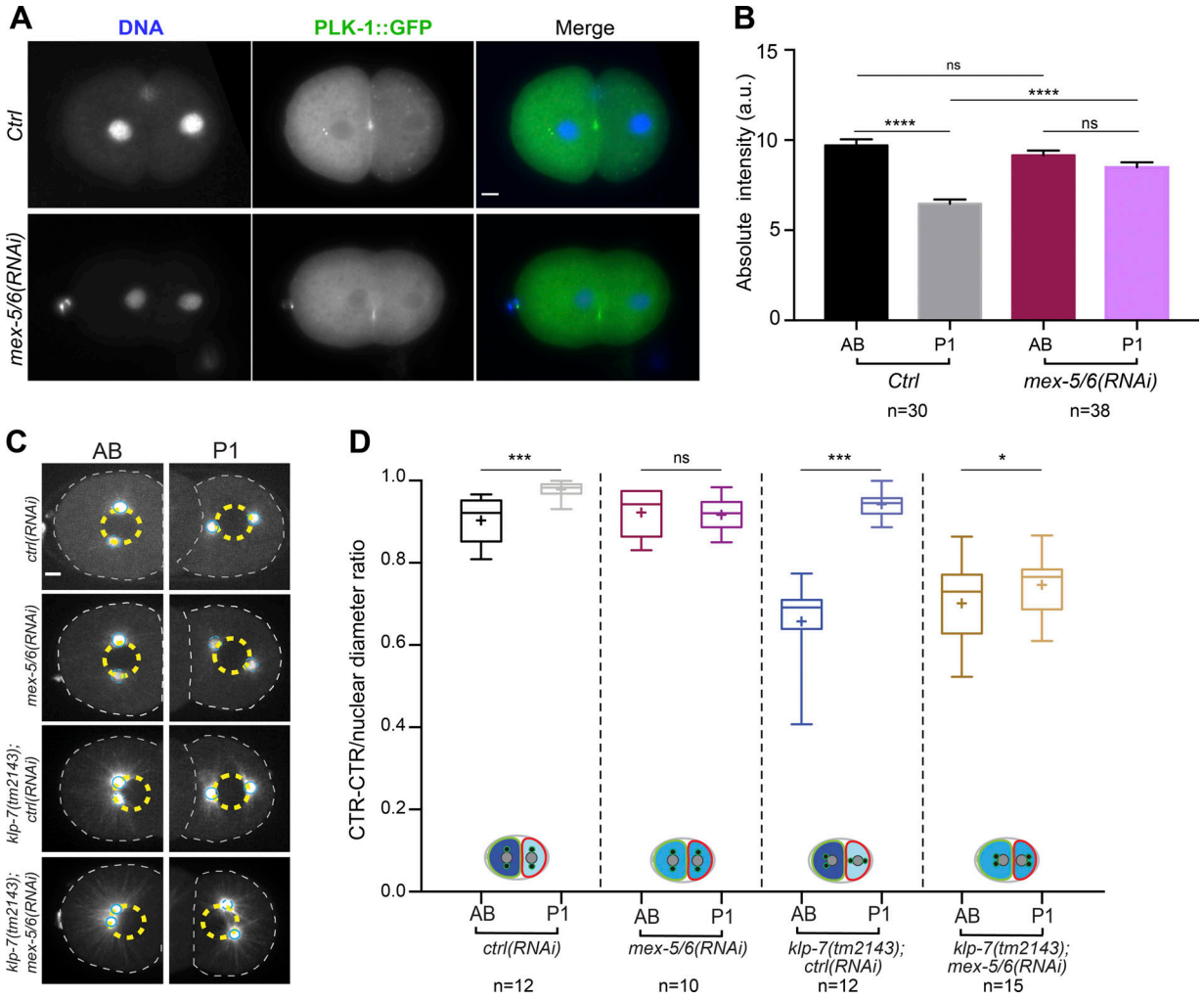

Figure 5. **Depletion of MEX-5/6 in the *klp-7(tm2143)* mutant results in centrosome separation defects in P1. (A)** Images of early fixed two-cell stage control and *mex-5/6(RNAi)* embryos expressing endogenously tagged PLK-1::GFP. **(B)** Absolute intensity quantification of PLK-1::GFP in control and *mex-5/6(RNAi)* AB and P1 cells. Errors bars indicate SEM. **(C)** Still images from time-lapse recording of AB and P1 cells from embryos treated with the indicated depletions. JDU316 (containing the *klp-7(tm2143)* deletion) and its parental strain, JCC483, were used in this experiment. **(D)** Quantification of the centrosome separation ratios of the indicated genotypes. Schematic models at the bottom indicate the polarity status (anterior = green; posterior = red) and the relative PLK-1 levels (high levels = dark blue; intermediate levels = blue; low levels = light blue). Scale bars, 5 µm. The number of cells/embryos analyzed is indicated at the bottom of the graph and the statistical test used is indicated in Table S1. *, P ≤ 0.05; ***, P ≤ 0.001; ****, P ≤ 0.001.

data confirmed that PLK-1 prevents the recruitment of LIN-5 at the cell cortex in the AB cell.

Discussion

Bipolar spindle assembly is an essential process that ensures faithful chromosome segregation. Here we show that this process is differentially controlled by cell polarity at the two-cell stage in *C. elegans* embryos. We show that centrosome separation initiation is delayed in the anterior AB cell compared with the posterior P1 cell, and that this difference is enhanced when the microtubule depolymerase KLP-7 is absent. Our data point to a model in which the polarity-dependent accumulation of PLK-1 in AB inhibits the cortical forces exerted via LIN-5 necessary to efficiently separate centrosomes in the absence of KLP-7 (Fig. 8).

Since AB is bigger than P1, the difference in centrosome separation behavior could depend on cell size. However, codepletion of Gα, a condition that abolishes the size difference without affecting polarity (Gotta and Ahringer, 2001), slowed down centrosome separation in both AB and P1 cells, but did not diminish the difference between both cells. This indicates that the asymmetric behavior of AB and P1 cells does not depend on cell size. Rather, our data point to the involvement of cell polarity: depletion of both PAR-3 and PAR-2 impaired centrosome separation in both AB and P1 in a *klp-7* mutant. This indicates that polarity controls this process, but rules out the antagonistic model of regulation between anterior and posterior PARs. Instead, we postulate that centrosome separation is controlled by PLK-1, a cytoplasmic factor asymmetrically enriched in the AB cell in a PAR-dependent manner (Budirahardja and Gönczy, 2008; Chase et al., 2000; Nishi et al., 2008; Rivers et al., 2008). Consistent with this model, low PLK-1 activity rescues the centrosome separation defect of KLP-7–depleted embryos; moreover, endogenous tagged PLK-1 is enriched in AB in WT

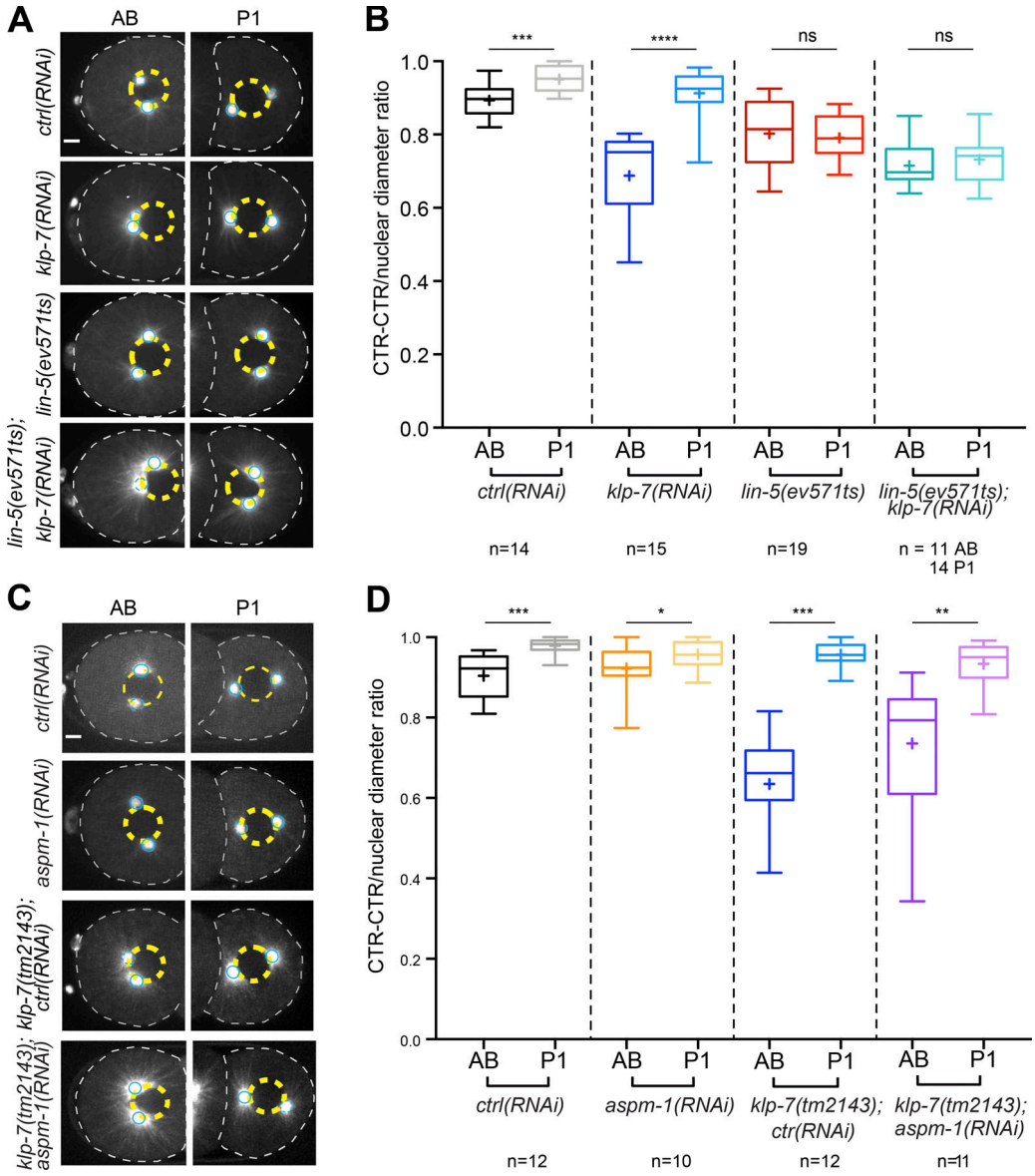

Figure 6. **A mutation in LIN-5 abolishes the difference of behavior of centrosomes in AB and P1 cells. (A)** Still images of AB and P1 cells taken from video recordings of embryos of the indicated genotypes. The FM102 strain containing the *lin-5(ev571ts)* mutation and its parental strain (AZ235) were used in this experiment. **(B)** Quantification of the centrosome separation ratios of the indicated genotypes. **(C)** Still images of AB and P1 cells from video recordings of JDU316 (containing the *klp-7(tm2143)* deletion) and its parental strain, JCC456, with the indicated genotypes. **(D)** Quantification of the centrosome separation ratios of the indicated genotypes. Scale bars, 5 µm. The number of cells/embryos analyzed is indicated at the bottom of the graph and the statistical test used is indicated in Table S1. *, P ≤ 0.05; **, P ≤ 0.01; ***, P ≤ 0.001; ****, P ≤ 0.001.

embryos, but its levels are intermediate in AB and P1 in PAR-3– and PAR-2–depleted embryos.

We note that the strength of the spindle assembly checkpoint, the main mitotic surveillance mechanism, is also regulated by cell lineage–specific mechanisms (Galli and Morgan, 2016; Gerhold et al., 2018). Combined with our findings, this indicates that the mitotic machinery in general is controlled not only by factors intrinsic to the mitotic spindle, but also by cell polarity (Fig. 8). We further note that in contrast to PAR-protein depletion, PLK-1 inactivation did not equalize centrosome separation in control embryos. Moreover, even in *klp-7* mutants, it did not fully equalize centrosome separation between AB and P1 cells. Since complete depletion of PLK-1 results in sterility, the difference in centrosome separation in *plk-1(or683ts)* embryos could be due to residual PLK-1 activity in these embryos. Alternatively, this may point to the existence of a pathway yet to be identified. Such a pathway would work via LIN-5, as LIN-5 depletion equalizes all conditions, but independently of PLK-1. We speculate that the fact that both the spindle assembly checkpoint and the forces that separate centrosomes are stronger in germ cell precursors could point to an evolutionary pressure that aims to ensure a higher fidelity in chromosome segregation in these cells. This difference cannot be major, though, since in live cell imaging

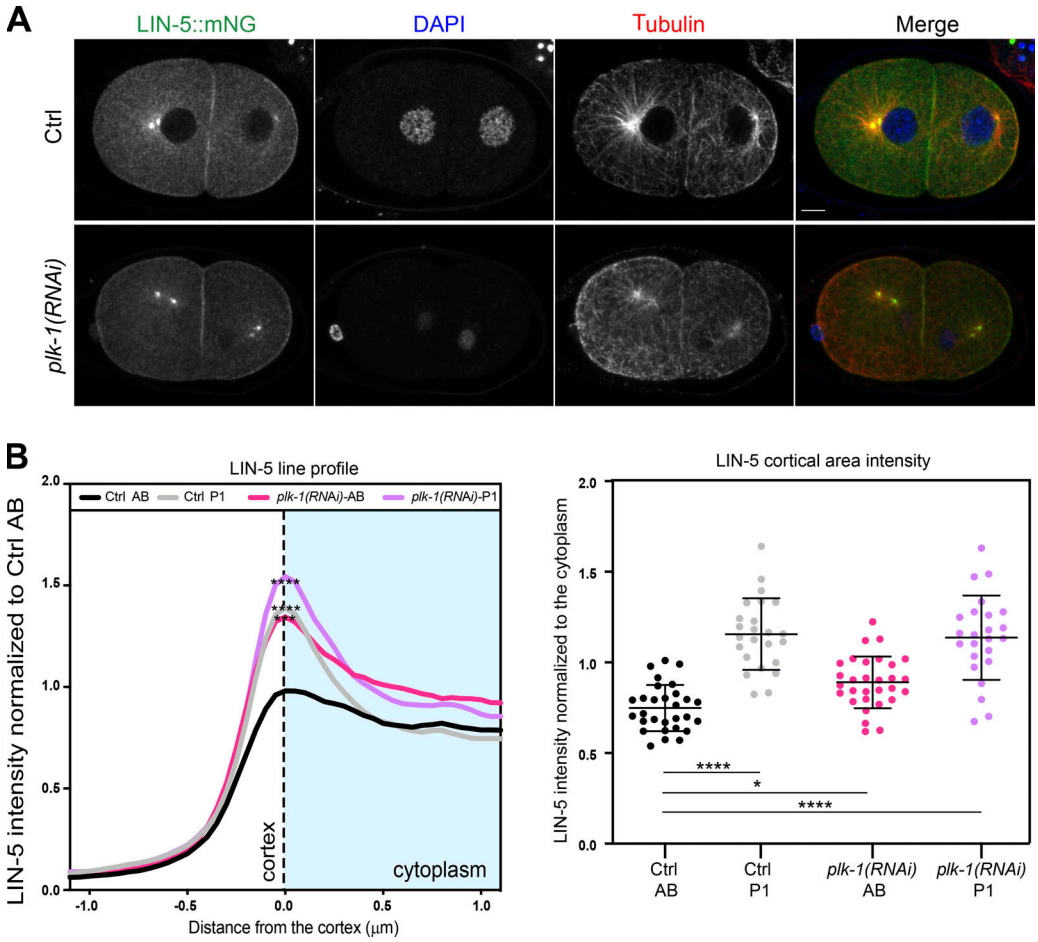

Figure 7. **PLK-1 limits LIN-5 cortical localization in AB. (A)** Confocal images of fixed early two-cell stage embryos expressing endogenously tagged LIN-5::mNG. LIN-5 is observed at the centrosomes, in the cytoplasm, and at the cell cortex. **(B)** Cortical LIN-5::mNG intensity profiles of AB and P1 cells in control and *plk-1(RNAi)* embryos. The line profile represents the mean intensities of 28 control and 29 *plk-1(RNAi)* embryos. In the line profile, the asterisks show the statistical difference compared with WT AB cells. **(C)** Quantifications of LIN-5::mNG intensities integrated over a cortical stripe after a Z projection in control and *plk-1(RNAi)* AB and P1 cells (see Materials and methods for details). Scale bar, 5 µm. The statistical test used is indicated in Table S1. *, P ≤ 0.05; ***, P ≤ 0.001; ****, P ≤ 0.001.

videos of two and four cell embryos expressing a histone mCherry marker, we could not detect major chromosome segregation defects after KLP-7 depletion (data not shown). We note that between 60% and 99% of KLP-7 mutant embryos die (Han et al., 2015; Connolly et al., 2015). However, whether this lethality is due to minor segregation defects in early

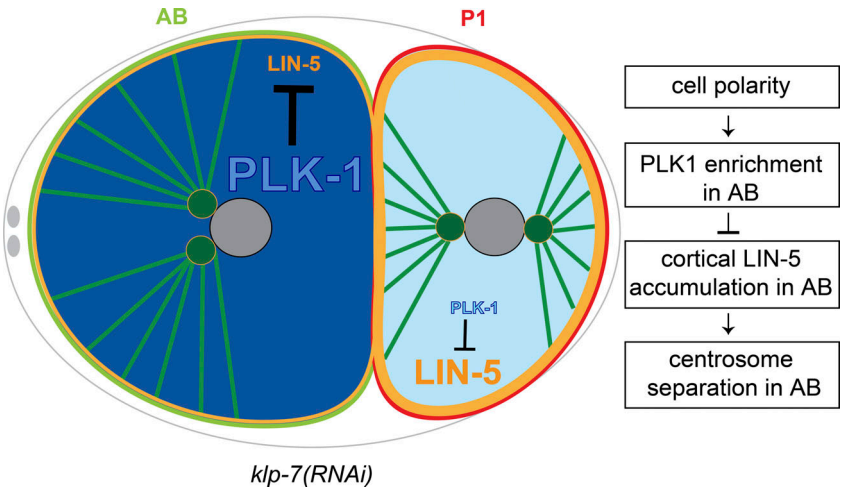

Figure 8. **Cell polarity modulates centrosomes separation in AB via PLK-1 and LIN-5.** Schematic representation of a KLP-7–depleted two-cell stage embryo consisting of an AB cell on the right with anterior PAR proteins at the cortex (green line) and a P1 cell on the left with the posterior PAR proteins at the cortex (red line). Nuclei are represented by gray circles, centrosomes by dark green spheres, and microtubules by green lines. PLK-1 is enriched in the AB cell (dark blue), resulting in low LIN-5 levels and activity (thin orange line) at the cortex. In contrast, in P1, low PLK-1 concentrations (light blue) allow LIN-5 to localize at the cortex (thick orange line) and exert a cortical pulling force, allowing the proper separation of the centrosomes.

embryos beyond the resolution of light microscopy or is caused by defects that arise later in development is unclear.

Our work identifies a key role for the microtubule depolymerase KLP-7 in promoting centrosome separation at the two-cell stage. How could it contribute to this process? We envisage several nonexclusive possibilities. First, KLP-7 might limit the number of inter-polar microtubules between the two centrosomes, which might exert a pulling force via minus end–directed kinesins (kinesin-14; Mountain et al., 1999). Second, KLP-7 might limit the number of astral microtubules that grow against the cell cortex and exert an inward-directed pushing force on the two centrosomes; alternatively, these astral microtubules might interact with the cortical actin network and thus generate a frictional force that slows down centrosome separation (Rosenblatt et al., 2004). The fact that KLP-7 depletion does not slow down centrosome migration around the nucleus but specifically delays their initial separation supports the first possibility without excluding a contribution from astral microtubules. Based on the fact that KLP-7 loss affected microtubule dynamics in both AB and P1, we postulate that its absence tends to prevent centrosome separation in both cells. While in P1 this force is mostly overcome by cortical LIN-5 (the P1 value in *klp-7* mutants is just statistically different from the control P1 value in some experiments), this does not occur in AB, due to the presence of PLK-1 (Fig. 8). Given that LIN-5 is a dynein-binding protein, we propose that dynein-based cortical pulling forces ensure an efficient initiation of centrosome separation in the absence of KLP-7. Interestingly, the different extents of LIN-5 cortical forces do not affect the maximal centrosome separation velocities, which could be limited by other factors, such as the centrosome-to-nucleus interactions or microtubule cross-linking activities. Consistent with a critical role of LIN-5, Gα depletion also reduces the extent of centrosome separation. Nevertheless, the *lin-5* mutant does not fully phenocopy Gα depletion in our assay, as in *lin-5* mutant embryos the difference in centrosome separation between AB and P1 is abolished. This difference between *Gα(RNAi)* and *lin-5(ev571ts)* embryos could be the result of a difference in penetrance between depletion of Gα by RNA interference and the *lin-5(ev571ts)* embryos. However, we find that *Gα(RNAi)* embryos divide in a symmetric manner, whereas the *lin-5(ev571ts)* embryos still maintain some asymmetry in size in the conditions used for our analysis. We therefore propose the existence of a cortical LIN-5 subpopulation that might not depend on Gα, consistent with human cell studies that identified Gα-independent NuMA pools (Kiyomitsu and Cheeseman, 2013; Kotak et al., 2014; Lee et al., 2018; Zheng et al., 2014). However, this LIN-5 population is regulated by PLK-1, which we find to prevent cortical LIN-5 recruitment in the AB cells. Given that PLK-1 has been shown to also target the human LIN-5 orthologue NuMA (Sana et al., 2018), we postulate that this regulatory step is conserved.

Overall, our study implies that centrosome separation is regulated in a tissue-dependent manner, and that one should not assume an ubiquitous regulation of this process. Therefore, it will be interesting to test whether this is also the case in human tissues, as suggested by the behavior of stem cell keratinocytes (Poulson and Lechler, 2010). This might be particularly relevant in the context of anti-cancer research, as centrosome separation is an attractive target for anti-mitotic drugs that can bypass the need of microtubule-targeting agents.

Materials and methods

Strains

The *C. elegans* strains used in this work are listed in Table S2. Worms were maintained using standard methods on nematode growth medium plates with OP50 bacteria (Brenner, 1974). Thermosensitive strains such as *plk-1(or683ts)*, *klp-7(or1092ts)*, *klp-7(or1292ts)*, *lin-5(ev571ts)*, and the mutant strain *klp-7(tm2143)* were maintained at 15°C. The rest of the fluorescent strains (see list in Table S2) were maintained between 22°C and 25°C. After double stranded RNA (dsRNA) injections, worms were incubated at the following temperatures: 25°C (Fig. 2, A–C; and Fig. 6, A and B), 22°C (Fig. 1, A and B; Fig. 4, D and E; Fig. 5, A and B; Fig. S1, D and E; Fig. S2, C and E; and Fig. S3), and 15°C (Fig. 3, B and C; Fig. 4, A and B; Fig. 5, C and D; Fig. 6, C and D; Fig. S1 C; and Fig. 4 C). With our conditions, the size of AB in the Gα depleted embryos was 51% egg length (AB/total egg length, n = 10), indicating that the depletion was efficient. The size of AB in the *lin-5(ev571ts)* embryos in our experimental conditions was 54.9% egg length (n = 10), suggesting only partial LIN-5 inactivation in the temperature-sensitive mutant.

RNA interference

dsRNA was produced in vitro using the clones from the Ahringer feeding library (Fraser et al., 2000; Kamath et al., 2003). The clones used in this study are listed in Table S2. For the control, we used the clone C06A6.2 previously found in the laboratory to have no effect on the early embryonic cell division and to be 100% viable. Each template was amplified by PCR using T7 primers, and dsRNA was produced using the Promega Ribomax RNA production system. dsRNA was injected in L4/young adult hermaphrodites. The incubation time of the injected worms before embryo dissection is listed in Table S2.

Live imaging of embryos

Gravid hermaphrodites were dissected on a coverslip into a drop of Egg Buffer (118 mM NaCl, 48 mM KCl, 2 mM $CaCl_2$, 2 mM $MgCl_2$, and 25 mM Hepes, pH 7.5). Embryos were mounted on a 2% agarose pad. Imaging was performed at room temperature (22–25°C) with a spinning disk microscope Zeiss Cell Observer.Z1 (inverted) equipped with HAL100 and HXP120 for transmission and fluorescence widefield visualization, a CSU X1 automatic Yokogowa spinning disk head, and a Plan Apo 63×/1.4 Oil DICIII objective. Images were acquired with an EMCCD camera (Evolve EM512 camera; Photometrics). Acquisition parameters were processed with MetaMorph or Visiview 4.00.10 software.

Fixation and immunostaining procedures

To stain *C. elegans* embryos, 15–20 gravid hermaphrodites were dissected in a drop of M9 (86 mM NaCl, 42 mM Na_2HPO_4, 22 mM KH_2PO_4, and 1 mM $MgSO_4$) on epoxy slides coated with 0.1% poly-L-lysine. A 22 × 40-mm coverslip was applied crosswise on

the square in order to squash the embryos, until the nuclei were almost transparent. The slides were transferred on a metal block on dry ice for 20 min or more, and the coverslip was removed before fixation. Immunostaining was performed as described in (Spilker et al., 2009). Briefly, embryos were fixed for 20 min in methanol, and placed for 20 min in a solution of PBS and 0.2% Tween (PBST), and BSA 1% to block the nonspecific antibody binding. The slides were incubated with primary antibodies overnight at 4°C. The following primary antibodies were used: anti-tubulin (mouse DM1A; Sigma-Aldrich; 1:1,000), anti KLP-7 (rabbit; used at 1 µg/µl; Gigant et al., 2017), and anti-LIN-5 (mouse; 1:2; Lorson et al., 2000). After three washes in PBST, slides were incubated for 45 min at 37°C with a solution containing secondary antibodies (Alexa Fluor 488–, 647–, and 568–coupled anti-rabbit or anti-mouse antibodies from Molecular Probes) and 1 mg/ml DAPI to visualize DNA. Slides were then washed three times in PBST before mounting using Mowiol (30% wt/vol glycerol, 3.87 mM Mowiol [Calbiochem, 475904], 0.2 M Tris, pH 8.5, and 0.1% DABCO).

To measure the levels of PLK-1::GFP, embryos were squashed and frozen as described above. After removal of the coverslip, slides were incubated 10 s in −20°C methanol and then transferred for 30 min in formaldehyde solution (1× PBS, 0.08 M Hepes, pH 6.9, 1.6 mM $MgSO_4$, 0.8 mM EDTA, 3.7% formaldehyde, and 1% Triton X-100). The samples were washed 3 × 15 min in PBS (1×) and were incubated with DAPI for 45 min at 37°C. Finally, after 3 × 5-min washes in PBS (1×), the slides were mounted in Mowiol.

Images were acquired with a Nikon Upright microscope Eclipse Ni-equipped with a 60×/0.5-1.25 Oil Iris Objective, a SOLA light engine (Lumencor), and DS-U3 Digital Camera Control unit (Nikon) controlled by NIS-elements BR4.30.02 software.

Image acquisition and analysis

Centrosomes tracking

4D video recordings of fluorescently labeled tubulin embryos were captured. The top and the bottom of the embryo were determined, and 1-µm Z stacks were taken every 15 s. Tracking of the centrosomes was performed using Imaris 7.7.1 64-bit software (Bitplane) with the spot tracking and measurement point tool. Two-cell–stage embryos with double nuclei were excluded from the analysis.

To measure the distance between the centrosomes over the time as shown in Fig. 2 D and Fig. 4 C, the centrosomes were tracked automatically with the spot tracking tool of Imaris software. Position X, Y, and Z of each centrosome was defined at each time point. To calculate the distance between the two centrosomes, we used the following formula: $AB=\sqrt{(xB - xA)^2 + (yB - yA)^2 + (zB - zA)^2}$. To calculate centrosome separation speeds, we plotted single-cell inter-centrosome distances and quantified based on the curve the centrosome separation velocities, when the two centrosomes separated at maximal speed (see Fig. S1 G). This occurred typically in the time frame when the inter-centrosome distance expanded from 4 to 11 µm (unless cells would undergo NEBD before, as was often the case in *klp-7* AB cells).

Microtubule dynamics at the cortex

EBP-2::GFP expressing embryos were imaged with the spinning disk microscope Zeiss Cell Observer.Z1 with an Apo 63×/1.4 Oil DICIII objective. To image EBP-2 comets, a single plane was taken at the embryo cortex. To stage the embryo, an image was taken in the middle plane of the embryo before and after recording the EBP-2 comets. Images were acquired at 400-ms intervals with a time exposure of 200 ms, without binning for 150 frames (1 min). EBP-2::GFP comets were counted in a semi-automatic way using Imaris 7.7.1 64-bit software. We calculated the number of frames from appearance to disappearance of EBP2::GFP comets.

Microtubule density at the cortex. The cortex of EBP2::GFP–expressing embryos was video-recorded. Images were taken every 400 ms with a time exposure of 200 ms. The comets were counted automatically for each time frame after image processing for a duration of 30 s. The source code is available on the GitHub website: https://github.com/LCirillo/FiJiMacro/blob/FiJiMacro/CometsQuantification.ijm.

Microtubule polymerization rate. Images were taken with at least one centrosome in the focal plane. Images were acquired every 200 ms, with a time exposure of 180 ms for a duration of 30 s. EBP2::GFP comets growing from the centrosome were tracked automatically using the spot tracking tool of the Imaris software. Only comets that could be followed for at least 10 frames were quantified.

Quantification of cytoplasmic PLK-1

Images were acquired with a Nikon Upright microscope Eclipse Ni-equipped with a 60×/0.5-1.25 Oil Iris Objective, a SOLA light engine (Lumencor), and a DS-U3 Digital Camera Control unit (Nikon) controlled by NIS-elements BR4.30.02 software. GFP signal was acquired with the SOLA light engine with a light power of 8% and was exposed for 300 ms.

Two squares with the same size (width = 6.30, height = 5.99, area = 37.711) were placed in AB and P1 cells. The absolute intensities were measured using ImageJ. The intensity values of the two squares were averaged for each AB and P1 cell.

LIN-5 cortical intensity measurement

Images for immunofluorescence of the LIN-5::mNG strain were acquired using an LSM800 Airyscan confocal microscope (Zeiss) equipped with two high-sensitive photomultiplier tube detectors. Experiments were performed with a Plan Apochromat 63× 1.40 NA oil objective. To acquire the LIN-5::mNG signal, a 488-nm 10-mW laser was used at 2.8% with a master gain of 620 and without binning. The middle plane of the embryo was set, and two stacks of 0.5 µm were taken above and below the middle plane. ZEN software (v.2.3; Zeiss) was used for the acquisition parameters.

LIN-5 levels were measured on two-cell embryos (at the stage shown in Fig. 7) using two methods. To obtain the line profile of cortical proteins shown in Fig. 7 B, a 10-pixel-wide × 3-µm-long line scan overlapping the cortex was used on the maximum projection of the five planes. For each embryo, the average of two line scans in AB and P1 was used for quantification. The line profiles of individual cells were normalized to the maximum

value of WT AB cells. For the quantification shown in Fig. 7 C, we created an ImageJ macro to calculate the mean gray value of a 16-µm-long line profile (https://github.com/LCirillo/FiJiMacro/blob/master/IJ_Macro_CorticalLin5). Briefly, after background subtraction and maximum projection of 5 z planes (0.5-µm step size), a 10-pixel-wide line was manually traced around the embryo cortex for both AB and P1. The point-by-point mean gray value was then averaged for a distance that spanned 8 µm from the center of the line profile in both directions. The value obtained was normalized on the cytoplasmic mean gray value of the corresponding cell, calculated on the same image, using a 90 × 90-pixel square. The data were analyzed using Python 3.7.0 and Prism 8 (GraphPad).

Statistical analysis

For the centrosome separation ratio analysis, to compare AB versus P1 of the same condition, we applied a paired *t* test (Wilcoxon test). To compare AB (or P1) of condition 1 to AB (or P1) of condition 2, we applied an unpaired multiple comparison test (Kruskal–Wallis). Statistical analysis was performed using the Prism software (7.02; GraphPad), which was also used to plot the graphs. Box plots show median, lower, and upper quartiles (line and box), minimum to maximum (whiskers), and means (+).

Online supplemental material

Fig. S1 shows the methodology of centrosome separation quantification and the extent of centrosome separation in different *klp-7* mutants at the two- and four-cell stage. Fig. S2 is a candidate-based screen for centrosome separation defects. Fig. S3 shows LIN-5 localization in *aspm-1* and *klp-7* mutants. Videos 1, 2, and 3 illustrate different centrosome separation defects. Table S1 documents all statistical analyses and Table S2 documents the strains and RNAi conditions used in this study.

Acknowledgments

We thank B. Bowerman (IBM, Eugene, OR), R. Gassmann (Instituto de Biologia Molecular e Celular, Porto, Portugal), L. Rose (University of California, Davis, Davis, CA), J. Dumont (Monod Institute, Paris, France), A. Sugimoto (Tohoku University, Sendai, Japan), A. Desai (University of California, San Diego, San Diego, CA), D.K. Cheerambathur (University of Edinburgh, Edinburgh, Scotland), and S. van den Heuvel (Utrecht University, Utrecht, Netherland) for strains and reagents. We also thank the Caenorhabditis Genetics Center (funded by the National Institutes of Health National Center for Research Resources) for strains. We thank Francois Prodon, Olivier Brun, and Nicolas Liaudet (Bio-imaging Core Facility) for support with image collection and analysis and Francoise Schwager for help with stainings and molecular biology. We also thank members of both the Meraldi and Gotta laboratories for fruitful discussions.

This work was supported by grants from the Swiss National Science Foundation to M. Gotta (31003A_156013 and 31003A_179413) and P. Meraldi (31003A_160006 and 31003A_175850) and from the University of Geneva.

The authors declare no competing financial interests.

Author contributions: The project was initiated and directed by P. Meraldi and M. Gotta. A. Bondaz performed all experiments. L. Cirillo wrote the codes to quantify microtubule dynamics at the cortex used in Fig. 2 B, Fig. 7 C, and Fig. S3 D. A. Bondaz, P. Meraldi, and M. Gotta analyzed and interpreted all the results and wrote the manuscript.

Submitted: 19 February 2019
Revised: 10 July 2019
Accepted: 6 September 2019

References

Bishop, J.D., Z. Han, and J.M. Schumacher. 2005. The Caenorhabditis elegans Aurora B kinase AIR-2 phosphorylates and is required for the localization of a BimC kinesin to meiotic and mitotic spindles. *Mol. Biol. Cell.* 16:742–756. https://doi.org/10.1091/mbc.e04-08-0682

Blangy, A., H.A. Lane, P. d'Hérin, M. Harper, M. Kress, and E.A. Nigg. 1995. Phosphorylation by p34cdc2 regulates spindle association of human Eg5, a kinesin-related motor essential for bipolar spindle formation in vivo. *Cell.* 83:1159–1169. https://doi.org/10.1016/0092-8674(95)90142-6

Brenner, S. 1974. The genetics of Caenorhabditis elegans. *Genetics.* 77:71–94.

Budirahardja, Y., and P. Gönczy. 2008. PLK-1 asymmetry contributes to asynchronous cell division of C. elegans embryos. *Development.* 135:1303–1313. https://doi.org/10.1242/dev.019075

Chase, D., C. Serafinas, N. Ashcroft, M. Kosinski, D. Longo, D.K. Ferris, and A. Golden. 2000. The polo-like kinase PLK-1 is required for nuclear envelope breakdown and the completion of meiosis in Caenorhabditis elegans. *Genesis.* 26:26–41.

Cheeks, R.J., J.C. Canman, W.N. Gabriel, N. Meyer, S. Strome, and B. Goldstein. 2004. C. elegans PAR proteins function by mobilizing and stabilizing asymmetrically localized protein complexes. *Curr. Biol.* 14:851–862. https://doi.org/10.1016/j.cub.2004.05.022

Connolly, A.A., K. Sugioka, C.-H. Chuang, J.B. Lowry, and B. Bowerman. 2015. KLP-7 acts through the Ndc80 complex to limit pole number in *C. elegans* oocyte meiotic spindle assembly. *J. Cell Biol.* 210:917–932. https://doi.org/10.1083/jcb.201412010

Couwenbergs, C., J.-C. Labbé, M. Goulding, T. Marty, B. Bowerman, and M. Gotta. 2007. Heterotrimeric G protein signaling functions with dynein to promote spindle positioning in *C. elegans*. *J. Cell Biol.* 179:15–22. https://doi.org/10.1083/jcb.200707085

Cuenca, A.A., A. Schetter, D. Aceto, K. Kemphues, and G. Seydoux. 2003. Polarization of the C. elegans zygote proceeds via distinct establishment and maintenance phases. *Development.* 130:1255–1265. https://doi.org/10.1242/dev.00284

De Simone, A., F. Nédélec, and P. Gönczy. 2016. Dynein Transmits Polarized Actomyosin Cortical Flows to Promote Centrosome Separation. *Cell Reports.* 14:2250–2262. https://doi.org/10.1016/j.celrep.2016.01.077

di Pietro, F., A. Echard, and X. Morin. 2016. Regulation of mitotic spindle orientation: an integrated view. *EMBO Rep.* 17:1106–1130. https://doi.org/10.15252/embr.201642292

Drechsler, H., T. McHugh, M.R. Singleton, N.J. Carter, and A.D. McAinsh. 2014. The Kinesin-12 Kif15 is a processive track-switching tetramer. *eLife.* 3:e01724. https://doi.org/10.7554/eLife.01724

Elbashir, S.M., J. Harborth, W. Lendeckel, A. Yalcin, K. Weber, and T. Tuschl. 2001. Duplexes of 21-nucleotide RNAs mediate RNA interference in cultured mammalian cells. *Nature.* 411:494–498. https://doi.org/10.1038/35078107

Fadero, T.C., T.M. Gerbich, K. Rana, A. Suzuki, M. DiSalvo, K.N. Schaefer, J.K. Heppert, T.C. Boothby, B. Goldstein, M. Peifer, et al. 2018. LITE microscopy: Tilted light-sheet excitation of model organisms offers high resolution and low photobleaching. *J. Cell Biol.* 217:1869–1882. https://doi.org/10.1083/jcb.201710087

Ferenz, N.P., A. Gable, and P. Wadsworth. 2010. Mitotic functions of kinesin-5. *Semin. Cell Dev. Biol.* 21:255–259. https://doi.org/10.1016/j.semcdb.2010.01.019

Fraser, A.G., R.S. Kamath, P. Zipperlen, M. Martinez-Campos, M. Sohrmann, and J. Ahringer. 2000. Functional genomic analysis of C. elegans

chromosome I by systematic RNA interference. *Nature.* 408:325–330. https://doi.org/10.1038/35042517

Galli, M., and D.O. Morgan. 2016. Cell Size Determines the Strength of the Spindle Assembly Checkpoint during Embryonic Development. *Dev. Cell.* 36:344–352. https://doi.org/10.1016/j.devcel.2016.01.003

Gerhold, A.R., V. Poupart, J.-C. Labbé, and P.S. Maddox. 2018. Spindle assembly checkpoint strength is linked to cell fate in the Caenorhabditis elegans embryo. *Mol. Biol. Cell.* 29:1435–1448. https://doi.org/10.1091/mbc.E18-04-0215

Gerson-Gurwitz, A., S. Wang, S. Sathe, R. Green, G.W. Yeo, K. Oegema, and A. Desai. 2016. A Small RNA-Catalytic Argonaute Pathway Tunes Germline Transcript Levels to Ensure Embryonic Divisions. *Cell.* 165:396–409. https://doi.org/10.1016/j.cell.2016.02.040

Gigant, E., M. Stefanutti, K. Laband, A. Gluszek-Kustusz, F. Edwards, B. Lacroix, G. Maton, J.C. Canman, J.P.I. Welburn, and J. Dumont. 2017. Inhibition of ectopic microtubule assembly by the kinesin-13 KLP-7 prevents chromosome segregation and cytokinesis defects in oocytes. *Development.* 144:1674–1686. https://doi.org/10.1242/dev.147504

Gotta, M., and J. Ahringer. 2001. Distinct roles for Galpha and Gbeta-gamma in regulating spindle position and orientation in Caenorhabditis elegans embryos. *Nat. Cell Biol.* 3:297–300. https://doi.org/10.1038/35060092

Grill, S.W., P. Gönczy, E.H. Stelzer, and A.A. Hyman. 2001. Polarity controls forces governing asymmetric spindle positioning in the Caenorhabditis elegans embryo. *Nature.* 409:630–633. https://doi.org/10.1038/35054572

Han, X., K. Adames, E.M.E. Sykes, and M. Srayko. 2015. The KLP-7 Residue S546 Is a Putative Aurora Kinase Site Required for Microtubule Regulation at the Centrosome in C. elegans. *PLoS One.* 10:e0132593. https://doi.org/10.1371/journal.pone.0132593

Heppert, J.K., A.M. Pani, A.M. Roberts, D.J. Dickinson, and B. Goldstein. 2018. A CRISPR Tagging-Based Screen Reveals Localized Players in Wnt-Directed Asymmetric Cell Division. *Genetics.* 208:1147–1164. https://doi.org/10.1534/genetics.117.300487

Hyman, A.A., and J.G. White. 1987. Determination of cell division axes in the early embryogenesis of Caenorhabditis elegans. *J. Cell Biol.* 105:2123–2135. https://doi.org/10.1083/jcb.105.5.2123

Kamath, R.S., A.G. Fraser, Y. Dong, G. Poulin, R. Durbin, M. Gotta, A. Kanapin, N. Le Bot, S. Moreno, M. Sohrmann, et al. 2003. Systematic functional analysis of the Caenorhabditis elegans genome using RNAi. *Nature.* 421:231–237. https://doi.org/10.1038/nature01278

Kapitein, L.C., E.J.G. Peterman, B.H. Kwok, J.H. Kim, T.M. Kapoor, and C.F. Schmidt. 2005. The bipolar mitotic kinesin Eg5 moves on both microtubules that it crosslinks. *Nature.* 435:114–118. https://doi.org/10.1038/nature03503

Kaseda, K., A.D. McAinsh, and R.A. Cross. 2012. Dual pathway spindle assembly increases both the speed and the fidelity of mitosis. *Biol. Open.* 1:12–18. https://doi.org/10.1242/bio.2011012

Kiyomitsu, T., and I.M. Cheeseman. 2013. Cortical dynein and asymmetric membrane elongation coordinately position the spindle in anaphase. *Cell.* 154:391–402. https://doi.org/10.1016/j.cell.2013.06.010

Kotak, S., C. Busso, and P. Gönczy. 2014. NuMA interacts with phosphoinositides and links the mitotic spindle with the plasma membrane. *EMBO J.* 33:1815–1830. https://doi.org/10.15252/embj.201488147

Lee, B.H., F. Schwager, P. Meraldi, and M. Gotta. 2018. p37/UBXN2B regulates spindle orientation by limiting cortical NuMA recruitment via PP1/Repo-Man. *J. Cell Biol.* 217:483–493. https://doi.org/10.1083/jcb.201707050

Lorson, M.A., H.R. Horvitz, and S. van den Heuvel. 2000. LIN-5 is a novel component of the spindle apparatus required for chromosome segregation and cleavage plane specification in *Caenorhabditis elegans*. *J. Cell Biol.* 148:73–86. https://doi.org/10.1083/jcb.148.1.73

Mardin, B.R., M. Isokane, M.R. Cosenza, A. Krämer, J. Ellenberg, A.M. Fry, and E. Schiebel. 2013. EGF-induced centrosome separation promotes mitotic progression and cell survival. *Dev. Cell.* 25:229–240. https://doi.org/10.1016/j.devcel.2013.03.012

Martino, L., S. Morchoisne-Bolhy, D.K. Cheerambathur, L. Van Hove, J. Dumont, N. Joly, A. Desai, V. Doye, and L. Pintard. 2017. Channel Nucleoporins Recruit PLK-1 to Nuclear Pore Complexes to Direct Nuclear Envelope Breakdown in C. elegans. *Dev. Cell.* 43:157–171.e7. https://doi.org/10.1016/j.devcel.2017.09.019

Mayer, T.U., T.M. Kapoor, S.J. Haggarty, R.W. King, S.L. Schreiber, and T.J. Mitchison. 1999. Small molecule inhibitor of mitotic spindle bipolarity identified in a phenotype-based screen. *Science.* 286:971–974. https://doi.org/10.1126/science.286.5441.971

Mazzorana, M., G. Montoya, and G.B. Mortuza. 2011. The centrosome: a target for cancer therapy. *Curr. Cancer Drug Targets.* 11:600–612. https://doi.org/10.2174/156800911795655949

McHedlishvili, N., S. Wieser, R. Holtackers, J. Mouysset, M. Belwal, A.C. Amaro, and P. Meraldi. 2012. Kinetochores accelerate centrosome separation to ensure faithful chromosome segregation. *J. Cell Sci.* 125:906–918. https://doi.org/10.1242/jcs.091967

Meraldi, P. 2016. Centrosomes in spindle organization and chromosome segregation: a mechanistic view. *Chromosome Res.* 24:19–34. https://doi.org/10.1007/s10577-015-9508-2

Mountain, V., C. Simerly, L. Howard, A. Ando, G. Schatten, and D.A. Compton. 1999. The kinesin-related protein, HSET, opposes the activity of Eg5 and cross-links microtubules in the mammalian mitotic spindle. *J. Cell Biol.* 147:351–366. https://doi.org/10.1083/jcb.147.2.351

Nguyen-Ngoc, T., K. Afshar, and P. Gönczy. 2007. Coupling of cortical dynein and G alpha proteins mediates spindle positioning in Caenorhabditis elegans. *Nat. Cell Biol.* 9:1294–1302. https://doi.org/10.1038/ncb1649

Nishi, Y., E. Rogers, S.M. Robertson, and R. Lin. 2008. Polo kinases regulate C. elegans embryonic polarity via binding to DYRK2-primed MEX-5 and MEX-6. *Development.* 135:687–697. https://doi.org/10.1242/dev.013425

Oegema, K., A. Desai, S. Rybina, M. Kirkham, and A.A. Hyman. 2001. Functional analysis of kinetochore assembly in *Caenorhabditis elegans*. *J. Cell Biol.* 153:1209–1226. https://doi.org/10.1083/jcb.153.6.1209

Park, D.H., and L.S. Rose. 2008. Dynamic localization of LIN-5 and GPR-1/2 to cortical force generation domains during spindle positioning. *Dev. Biol.* 315:42–54. https://doi.org/10.1016/j.ydbio.2007.11.037

Poulson, N.D., and T. Lechler. 2010. Robust control of mitotic spindle orientation in the developing epidermis. *J. Cell Biol.* 191:915–922. https://doi.org/10.1083/jcb.201008001

Raaijmakers, J.A., R.G.H.P. van Heesbeen, J.L. Meaders, E.F. Geers, B. Fernandez-Garcia, R.H. Medema, and M.E. Tanenbaum. 2012. Nuclear envelope-associated dynein drives prophase centrosome separation and enables Eg5-independent bipolar spindle formation. *EMBO J.* 31:4179–4190. https://doi.org/10.1038/emboj.2012.272

Rattner, J.B., and M.W. Berns. 1976. Centriole behavior in early mitosis of rat kangaroo cells (PTK2). *Chromosoma.* 54:387–395. https://doi.org/10.1007/BF00292817

Rivers, D.M., S. Moreno, M. Abraham, and J. Ahringer. 2008. PAR proteins direct asymmetry of the cell cycle regulators Polo-like kinase and Cdc25. *J. Cell Biol.* 180:877–885. https://doi.org/10.1083/jcb.200710018

Rose, L., and P. Gönczy. 2014. Polarity establishment, asymmetric division and segregation of fate determinants in early C. elegans embryos. *WormBook.* Dec 30:1–43. https://doi.org/10.1895/wormbook.1.30.2

Rosenblatt, J. 2005. Spindle assembly: asters part their separate ways. *Nat. Cell Biol.* 7:219–222. https://doi.org/10.1038/ncb0305-219

Rosenblatt, J., L.P. Cramer, B. Baum, and K.M. McGee. 2004. Myosin II-dependent cortical movement is required for centrosome separation and positioning during mitotic spindle assembly. *Cell.* 117:361–372. https://doi.org/10.1016/S0092-8674(04)00341-1

Sana, S., R. Keshri, A. Rajeevan, S. Kapoor, and S. Kotak. 2018. Plk1 regulates spindle orientation by phosphorylating NuMA in human cells. *Life Sci. Alliance.* 1:e201800223. https://doi.org/10.26508/lsa.201800223

Saunders, A.M., J. Powers, S. Strome, and W.M. Saxton. 2007. Kinesin-5 acts as a brake in anaphase spindle elongation. *Curr. Biol.* 17:R453–R454. https://doi.org/10.1016/j.cub.2007.05.001

Schubert, C.M., R. Lin, C.J. de Vries, R.H. Plasterk, and J.R. Priess. 2000. MEX-5 and MEX-6 function to establish soma/germline asymmetry in early C. elegans embryos. *Mol. Cell.* 5:671–682. https://doi.org/10.1016/S1097-2765(00)80246-4

Segbert, C., R. Barkus, J. Powers, S. Strome, W.M. Saxton, and O. Bossinger. 2003. KLP-18, a Klp2 kinesin, is required for assembly of acentrosomal meiotic spindles in Caenorhabditis elegans. *Mol. Biol. Cell.* 14:4458–4469. https://doi.org/10.1091/mbc.e03-05-0283

Silkworth, W.T., I.K. Nardi, R. Paul, A. Mogilner, and D. Cimini. 2012. Timing of centrosome separation is important for accurate chromosome segregation. *Mol. Biol. Cell.* 23:401–411. https://doi.org/10.1091/mbc.e11-02-0095

Spilker, A.C., A. Rabilotta, C. Zbinden, J.-C. Labbé, and M. Gotta. 2009. MAP kinase signaling antagonizes PAR-1 function during polarization of the early Caenorhabditis elegans embryo. *Genetics.* 183:965–977. https://doi.org/10.1534/genetics.109.106716

Srayko, M., A. Kaya, J. Stamford, and A.A. Hyman. 2005. Identification and characterization of factors required for microtubule growth and nucleation in the early C. elegans embryo. *Dev. Cell.* 9:223–236. https://doi.org/10.1016/j.devcel.2005.07.003

Sulston, J.E., E. Schierenberg, J.G. White, and J.N. Thomson. 1983. The embryonic cell lineage of the nematode Caenorhabditis elegans. *Dev. Biol.* 100:64–119. https://doi.org/10.1016/0012-1606(83)90201-4

Tanenbaum, M.E., L. Macůrek, A. Janssen, E.F. Geers, M. Alvarez-Fernández, and R.H. Medema. 2009. Kif15 cooperates with eg5 to promote bipolar spindle assembly. *Curr. Biol.* 19:1703–1711. https://doi.org/10.1016/j.cub.2009.08.027

Toso, A., J.R. Winter, A.J. Garrod, A.C. Amaro, P. Meraldi, and A.D. McAinsh. 2009. Kinetochore-generated pushing forces separate centrosomes during bipolar spindle assembly. *J. Cell Biol.* 184:365–372. https://doi.org/10.1083/jcb.200809055

Vaisberg, E.A., M.P. Koonce, and J.R. McIntosh. 1993. Cytoplasmic dynein plays a role in mammalian mitotic spindle formation. *J. Cell Biol.* 123:849–858. https://doi.org/10.1083/jcb.123.4.849

van der Voet, M., C.W.H. Berends, A. Perreault, T. Nguyen-Ngoc, P. Gönczy, M. Vidal, M. Boxem, and S. van den Heuvel. 2009. NuMA-related LIN-5, ASPM-1, calmodulin and dynein promote meiotic spindle rotation independently of cortical LIN-5/GPR/Galpha. *Nat. Cell Biol.* 11:269–277. https://doi.org/10.1038/ncb1834

van Heesbeen, R.G.H.P., M.E. Tanenbaum, and R.H. Medema. 2014. Balanced activity of three mitotic motors is required for bipolar spindle assembly and chromosome segregation. *Cell Reports.* 8:948–956. https://doi.org/10.1016/j.celrep.2014.07.015

van Heesbeen, R.G.H.P., J.A. Raaijmakers, M.E. Tanenbaum, V.A. Halim, D. Lelieveld, C. Lieftink, A.J.R. Heck, D.A. Egan, and R.H. Medema. 2017. Aurora A, MCAK, and Kif18b promote Eg5-independent spindle formation. *Chromosoma.* 126:473–486. https://doi.org/10.1007/s00412-016-0607-4

Vanneste, D., M. Takagi, N. Imamoto, and I. Vernos. 2009. The role of Hklp2 in the stabilization and maintenance of spindle bipolarity. *Curr. Biol.* 19:1712–1717. https://doi.org/10.1016/j.cub.2009.09.019

Waters, J.C., R.W. Cole, and C.L. Rieder. 1993. The force-producing mechanism for centrosome separation during spindle formation in vertebrates is intrinsic to each aster. *J. Cell Biol.* 122:361–372. https://doi.org/10.1083/jcb.122.2.361

Zheng, Z., Q. Wan, G. Meixiong, and Q. Du. 2014. Cell cycle-regulated membrane binding of NuMA contributes to efficient anaphase chromosome separation. *Mol. Biol. Cell.* 25:606–619. https://doi.org/10.1091/mbc.e13-08-0474